Improved method for calibrating a Stokes polarimeter

Bruno Boulbry,[1] Jessica C. Ramella-Roman,[2] and Thomas A. Germer[1,*]

[1]Optical Technology Division, National Institute of Standards and Technology, Gaithersburg, Maryland 20886, USA
[2]Department of Biomedical Engineering, The Catholic University of America, Washington, D.C. 20064, USA

*Corresponding author: germer@nist.gov

Received 13 July 2007; revised 28 September 2007; accepted 3 October 2007;
posted 13 November 2007 (Doc. ID 85228); published 7 December 2007

We present a method for calibrating a polarization state analyzer that uses a set of well-characterized reference polarization states and makes no assumptions about the optics contained in the polarimeter other than their linearity. The method requires that a matrix be constructed that contains the data acquired for each of the reference polarization states and that this matrix be pseudoinverted. Since this matrix is usually singular, we improve the method by performing the pseudoinversion by singular value decomposition, keeping only the four largest singular values. We demonstrate the calibration technique using an imaging polarimeter based upon liquid crystal variable retarders and with light emitting diode (LED) illumination centered at 472 nm, 525 nm, and 630 nm. We generate the reference polarization states by using an unpolarized source, a single polarizer, and a Fresnel rhomb. This method is particularly useful when calibrations are performed on field-grade instruments at a centrally maintained facility and when a traceability chain needs to be maintained.

OCIS codes: 120.2130, 120.5410, 260.5430.

1. Introduction

Mueller-matrix polarimeters (sample-measuring polarimeters) or Stokes-vector polarimeters (light-measuring polarimeters) have been widely used to measure different polarization properties in optical systems and samples [1,2]. Recently, there have been numerous applications of polarized light including the analysis of polarized light for determining the thickness and refractive index of thin surface films [3], solar astronomy [4], remote sensing (underwater surveying, for example [5,6]), telecommunication systems [7,8], and biology and medicine [9,10]. Imaging polarimetry has also emerged in the last few years to enhance conventional imagery, by providing insightful understanding of the elements that constitute the object based on its polarimetric properties such as birefringence, dichroism, and depolarizing properties [11,12]. Imaging polarimetry is particularly useful to probe the constituent element organization in biological tissues [13]. Spectroscopic polarimeters combine the information available to spectral sensing techniques with polarization [14]. While the spectral information distinguishes materials, polarization information tells us about surface or subsurface features, shape, and roughness [15].

An issue that arises with polarimeters is their proper calibration. Building a Stokes polarimeter with optimal components is often costly, and that cost can often be alleviated by reducing the performance specifications on the components and improving the method by which the polarimeter is calibrated. In this paper, we describe a calibration procedure that makes no assumptions about the components making up the polarimeter other than that there is a linear transformation between a set of measurements and the Stokes vector. The procedure requires a set of reference polarization states that can be traceable to a centrally maintained reference. The method also yields improved resistance to statistical sources of noise during both the calibration procedure and the subsequent measurement.

This paper is organized as follows. First, in Section 2, we review the principles of polarimetry using a data reduction matrix. Next, in Sections 3 and 4, we describe two methods for calibrating polarimeters, the second one being more general. In Section 5, we describe the polarimeter that we use to demonstrate the calibration methods. We then describe a reference

0003-6935/07/358533-09$15.00/0

polarization state generator in Section 6. We present the results for the calibration in Section 7. In Section 8, we give a brief description of the main uncertainties that arise during the improved calibration procedure. Finally, we summarize our results in Section 9.

2. Principles of Measurements

A Stokes vector polarimeter completely or partially measures the Stokes vector of light. The Stokes vector describes the time-averaged polarization properties of an electromagnetic field and is defined as

$$\mathbf{S} = \begin{pmatrix} S_0 \\ S_1 \\ S_2 \\ S_3 \end{pmatrix} = \begin{pmatrix} I_x + I_y \\ I_x - I_y \\ I_{45^\circ} - I_{-45^\circ} \\ I_{\mathrm{rcp}} - I_{\mathrm{lcp}} \end{pmatrix}, \tag{1}$$

where I_j represents the intensity in polarization state j. The subscript j indicates that only that part which is polarized in a particular direction is considered, with lcp and rcp standing for left- and right-circular polarization, respectively. Because of the nature of $\mathbf{S}$, the Stokes parameters cannot be measured directly; they must be computed from a set of measurements through polarization analyzers. A straightforward method is to measure four linearly polarized intensities through a linear analyzer at 0°, 45°, 90°, and 135° and through a left- and a right-circular analyzer [15]. The Stokes elements could then be evaluated following the definition of the Stokes vector in Eq. (1). In matrix form, Eq. (1) may be written as

$$\mathbf{S} = \mathbf{W} \cdot \mathbf{I}, \tag{2}$$

where

$$\mathbf{I} = (I_x \quad I_y \quad I_{45^\circ} \quad I_{-45^\circ} \quad I_{\mathrm{rcp}} \quad I_{\mathrm{lcp}})^T \tag{3}$$

is a vector containing the six measured intensities, and

$$\mathbf{W} = \begin{pmatrix} 1 & 1 & 0 & 0 & 0 & 0 \\ 1 & -1 & 0 & 0 & 0 & 0 \\ 0 & 0 & 1 & -1 & 0 & 0 \\ 0 & 0 & 0 & 0 & 1 & -1 \end{pmatrix} \tag{4}$$

is referred to as the data reduction matrix. Since

$$I_x + I_y = I_{45^\circ} + I_{-45^\circ} = I_{\mathrm{rcp}} + I_{\mathrm{lcp}}, \tag{5}$$

the matrix $\mathbf{W}$ is not unique. That is, specific combinations of the measured intensities should be zero. Consequently, by adding such a quantity, e.g., $-\frac{2}{3}I_x - \frac{2}{3}I_y + \frac{1}{3}I_{45^\circ} + \frac{1}{3}I_{-45^\circ} + \frac{1}{3}I_{\mathrm{rcp}} + \frac{1}{3}I_{\mathrm{lcp}} = 0$, to each row of Eq. (1), we can generate another matrix

$$\mathbf{W} = \begin{pmatrix} 1/3 & 1/3 & 1/3 & 1/3 & 1/3 & 1/3 \\ 1/3 & -5/3 & 1/3 & 1/3 & 1/3 & 1/3 \\ -2/3 & -2/3 & 4/3 & -2/3 & 1/3 & 1/3 \\ -2/3 & -2/3 & 1/3 & 1/3 & 4/3 & -2/3 \end{pmatrix} \tag{6}$$

that will also yield the same result for intensity measurements that satisfy Eq. (5). The difference between the matrices in Eqs. (4) and (6) is how they weigh the different intensity measurements and thus how uncertainties will propagate. If the uncertainty in each of the measurements of intensity is s, then propagation of uncertainties, which is achieved by taking the square root of the sum of squares of each row of each matrix, will yield an uncertainty in the measured Stokes vector of

$$u_s = (1.414s,\ 1.414s,\ 1.414s,\ 1.414s)^T \tag{7}$$

for the first matrix and

$$u_s = (0.816s,\ 1.826s,\ 1.826s,\ 1.826s)^T \tag{8}$$

for the second matrix. Thus, the choice of using the first row of the matrix in Eq. (6) and the second three rows of the matrix in Eq. (4) provides a lower uncertainty for all Stokes vector elements, yielding

$$\mathbf{W} = \begin{pmatrix} 1/3 & 1/3 & 1/3 & 1/3 & 1/3 & 1/3 \\ 1 & -1 & 0 & 0 & 0 & 0 \\ 0 & 0 & 1 & -1 & 0 & 0 \\ 0 & 0 & 0 & 0 & 1 & -1 \end{pmatrix}. \tag{9}$$

The matrix in Eq. (9) can be shown to be the optimum matrix by evaluating its condition number [16]. The higher the condition number, the less linearly independent are the columns or rows of $\mathbf{W}$. Minimizing the condition number maximizes the relative importance of each of the measurements, increasing system stability and decreasing noise propagation. Tyo demonstrated that the minimum condition number for $\mathbf{W}$ is $\sqrt{3}$ [17], which is that of the matrix in Eq. (9).

3. Old Calibration Method

A Stokes vector polarimeter is typically composed of a collection of retarders and polarizers that are cascaded to form a polarization state analyzer. The components are modulated, either by rotating one or more of them or by varying their retardance, and signals are acquired for N configurations. The Stokes vector $\mathbf{S}_i$ of the light reaching the detector when the analyzer is in configuration i is

$$\mathbf{S}_i = \mathbf{M}_i \cdot \mathbf{S}, \tag{10}$$

where $\mathbf{M}_i$ is the Mueller matrix of the respective analyzer. The measured intensity I_i is the first term of $\mathbf{S}_i$ and can be expressed as a function of the four unknown components,

$$I_i = \mathbf{S}_{\text{sense},i} \cdot \mathbf{S}, \tag{11}$$

where we define a Stokes sensitivity vector, consisting of the first row of $\mathbf{M}_i$,

$$\mathbf{S}_{\text{sense},i} = (M_{i,00} \quad M_{i,01} \quad M_{i,02} \quad M_{i,03}). \tag{12}$$

If we define a matrix $\mathbf{A}$ to contain the Stokes sensitivities for each of the configurations of the polarimeter, then the intensity vector for an unknown Stokes vector is

$$\mathbf{I} = \mathbf{A} \cdot \mathbf{S}, \tag{13}$$

where

$$\mathbf{A} = \begin{pmatrix} M_{1,00} & M_{1,01} & M_{1,02} & M_{1,03} \\ \vdots & \vdots & \vdots & \vdots \\ M_{N,00} & M_{N,01} & M_{N,02} & M_{N,03} \end{pmatrix}. \tag{14}$$

Finally, we can then find $\mathbf{W}$ by solving for $\mathbf{S}$ in Eq. (13). That is, $\mathbf{W}$ is given by the left pseudoinverse of $\mathbf{A}$:

$$\mathbf{W} = (\mathbf{A}^T \cdot \mathbf{A})^{-1} \cdot \mathbf{A}^T. \tag{15}$$

Unfortunately, this method requires each of the Stokes sensitivities [Eq. (11)] to be known. A conventional method to calibrate such a system is to assume a parameterization for each optical element. For example, for a retarder, one will assume it is fully characterized by a retardance and an orientation. A regression analysis is then performed on a set of calibration data. Optical devices and their physical orientation, however, are never perfect. Some physical effects, such as multiple reflections between or within optical devices, incorrectly oriented crystals in retarders, imperfect polarizers, and residual birefringence, will often cause the Mueller matrices of the analyzer components to deviate from the ideal, and moreover, will cause them to deviate from what has been parameterized [18,19]. For field instruments, obtaining high quality components to alleviate these concerns adds to their price, substantially.

4. New Calibration Method

In this section we describe a procedure that can be used to calibrate any Stokes polarimeter, without requiring knowledge of the details of the components making up that polarimeter. We assume that the polarimeter measures N intensities corresponding to the N different configurations of the analyzing elements. The matrix $\mathbf{W}$ is thus of dimension $4 \times N$. To calibrate the polarimeter, let us assume we can generate M different reference polarization states, for which we know the Stokes vectors $\mathbf{S}_i (i = 1, \ldots, M)$. We thus know that

$$[\mathbf{S}_1 \quad \mathbf{S}_1 \quad \cdots \quad \mathbf{S}_M] = \mathbf{W} \cdot [\mathbf{I}_1 \quad \mathbf{I}_2 \quad \cdots \quad \mathbf{I}_M] \tag{16}$$

should hold, where $\mathbf{I}_i$ is the vector containing the N measurements for the ith Stokes vector. We can rewrite Eq. (16) as

$$\mathbf{S} = \mathbf{W} \cdot \mathbf{I}, \tag{17}$$

where $\mathbf{S} = [\mathbf{S}_1 \quad \mathbf{S}_2 \quad \ldots \quad \mathbf{S}_M]$ is a $4 \times M$ matrix, and $\mathbf{I} = [\mathbf{I}_1 \quad \mathbf{I}_2 \quad \ldots \quad \mathbf{I}_M]$ is a $N \times M$ matrix. The data reduction matrix $\mathbf{W}$ can then be determined by the right pseudoinverse of $\mathbf{I}$:

$$\mathbf{W} = \mathbf{S} \cdot \mathbf{I}^{-1}. \tag{18}$$

The right pseudoinverse of $\mathbf{I}$ can be determined from

$$\mathbf{I}^+ = \mathbf{I}^T \cdot (\mathbf{I} \cdot \mathbf{I}^T)^{-1}. \tag{19}$$

However, one must be careful when using Eq. (19) because the matrix $\mathbf{I} \cdot \mathbf{I}^T$ is not well conditioned, and pseudoinversion can lead to large variations in the resulting matrix $\mathbf{W}$. That is, while $\mathbf{I}$ is an $N \times M$ matrix, we will show below that theoretically (in the limit of no measurement errors) it has only four nonzero singular values. The variations that occur are a manifestation of the nonuniqueness of $\mathbf{W}$, seen above in Eqs. (4) and (6). While the resulting matrix may function as expected, it cannot be easily compared to the ideal matrix, and the uncertainties in subsequent measurements may not be optimized.

A solution to this problem consists of using the singular value decomposition (SVD) to calculate the pseudoinverse of $\mathbf{I}$ [20]. The SVD decomposes any matrix $\mathbf{I}$ into the product of two real orthonormal matrices, $\mathbf{U}$ (of dimension $N \times N$) and $\mathbf{V}$ (of dimension $M \times M$), and a diagonal real matrix $\mathbf{D}$ (of dimension $N \times M$), such that

$$\mathbf{I} = \mathbf{U} \cdot \mathbf{D} \cdot \mathbf{V}^T. \tag{20}$$

By convention, the diagonal elements σ_i of $\mathbf{D}$, which are referred to as the singular values of $\mathbf{I}$, are nonnegative and sorted in decreasing order, i.e., $\sigma_1 \geq \sigma_2 \geq \ldots \geq \sigma_p \geq 0$; this convention makes the SVD unique except when one or more singular values occur with multiplicity greater than one (in which case the corresponding columns of $\mathbf{U}$ and $\mathbf{V}$ can be replaced by linear combinations of themselves). An important property of the SVD is that it explicitly constructs orthonormal bases for the range and the nullspace of $\mathbf{I}$. Specifically, the columns of $\mathbf{U}$ whose same-numbered elements σ_i are nonzero are an orthonormal set of basis vectors that span the range; the columns of $\mathbf{V}$ whose same-numbered elements are zero are an orthonormal basis for the nullspace [21].

To determine the number of nonzero singular values of $\mathbf{I}$, consider that it contains columns consisting of the measured intensities for a set of Stokes vectors having four degrees of freedom. It is thus obvious that if the input Stokes vectors span all four dimensions,

then the range of $\mathbf{I}$ should have four dimensions. Thus, $\mathbf{I}$ should only have four nonzero singular values.

One advantage of the SVD is that the pseudoinverse of the matrix can be determined from

$$\mathbf{I}^{+} = \mathbf{V} \cdot \mathrm{diag}(1/\sigma_1, \ldots, 1/\sigma_N) \cdot \mathbf{U}^{T}. \tag{21}$$

If the matrix is singular, then the inverse of any zero singular value is set to zero. In practice, with random errors introduced into the measurement, the matrix $\mathbf{I}$ has N nonzero singular values, yet all but four of them are very small. We argue that these small singular values should be treated as zero, since otherwise their effect on the pseudoinverse is very large, yet their significance is negligible. They exist to reproduce the noise in the calibration measurement and to span the space of nonoptimal matrices. Thus, we use the truncated pseudoinverse

$$\hat{\mathbf{I}}^{+} = \mathbf{V} \cdot \mathrm{diag}(1/\sigma_1, \ldots, 1/\sigma_4, \ \ 0, \ldots, 0) \cdot \mathbf{U}^{T} \tag{22}$$

and let

$$\mathbf{W} = \mathbf{S} \cdot \hat{\mathbf{I}}^{+}. \tag{23}$$

As we will demonstrate later, the effect of using the truncated pseudoinverse is that the data reduction matrix is stable, optimized, and less susceptible to measurement uncertainties.

5. Polarimeter

We have constructed and operated a spectroscopic Stokes polarimeter using a pair of liquid-crystal (LC) devices in combination with a polarizer [22], shown schematically in the bottom frame of Fig. 1. The LC devices act as uniaxial variable retarders, with their retardance being controlled by an external applied voltage. One of the main interests of using these devices is that they can be switched at near-video frame rates for imaging applications [23]. In addition, they do not require any moving parts, have large acceptance angles, and have large clear apertures.

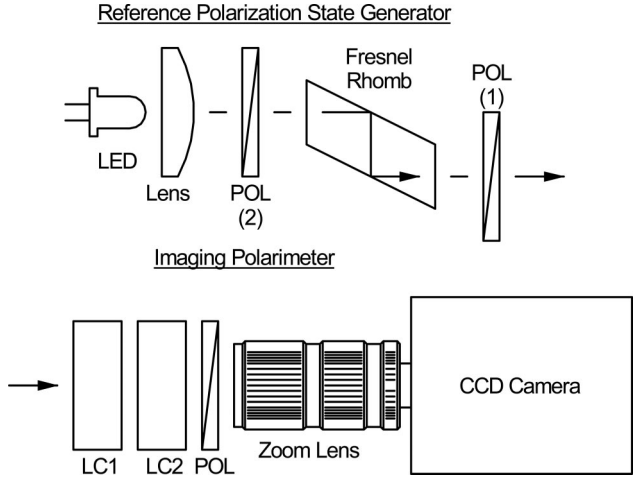

Fig. 1. Reference polarization state generator (bottom) and the imaging polarimeter (top). The polarizer (POL) in the reference polarization state generator is placed in positions 1 and 2 for the two configurations.

In our measurements the fast axes of the LC retarders were nominally oriented at the fixed angles $\theta_1 = 0°$ and $\theta_2 = -45°$ with respect to the polarizer, and the nominal retardance combinations were varied according to $(\delta_1, \delta_2) = (\delta_1^{a}, \delta_2^{a})$, $(\delta_1^{a}, \delta_2^{c})$, $(\delta_1^{b}, \delta_2^{d})$, $(\delta_1^{b}, \delta_2^{b})$, $(\delta_1^{a}, \delta_2^{b})$, and $(\delta_1^{a}, \delta_2^{d})$, where $\delta_1^{a} = 0$, $\delta_1^{b} = -90°$, $\delta_2^{a} = 0$, $\delta_2^{b} = -90°$, $\delta_2^{c} = -180°$, and $\delta_2^{d} = -270°$. The voltages applied to the LC retarders to get the desired retardance were calculated using calibration data provided by the manufacturer. Since the manufacturer only provided data for a single wavelength ($\lambda = 633$ nm), data for other wavelengths were determined by assuming that the devices had no dispersion.

Ideally, the Mueller matrix for the analyzer is

$$\mathbf{M} = \mathbf{M}_{\mathrm{pol}}(\theta_3) \cdot \mathbf{M}_{\mathrm{ret}}(\theta_2, \ \delta_2) \cdot \mathbf{M}_{\mathrm{ret}}(\theta_1, \ \delta_1), \tag{24}$$

where $\mathbf{M}_{\mathrm{pol}}(\theta)$ is the Mueller matrix for a linear polarizer at angle θ, and $\mathbf{M}_{\mathrm{ret}}(\theta, \delta)$ is the Mueller matrix for a linear retarder with retardance δ oriented with its fast axis at angle θ. Using the nominal values of the retardances and their orientations, the nominal analysis matrix is

$$\mathbf{A} = \begin{pmatrix} 1 & 1 & 0 & 0 \\ 1 & -1 & 0 & 0 \\ 1 & 0 & 1 & 0 \\ 1 & 0 & -1 & 0 \\ 1 & 0 & 0 & 1 \\ 1 & 0 & 0 & -1 \end{pmatrix}. \tag{25}$$

The detector consisted of a 12-bit digital charge-coupled device (CCD) camera with a zoom lens. For the calibration of this instrument, a diffuser was placed between the polarizer and the front of the zoom lens, so that the camera was effectively being used as an integrating, nonimaging detector. The signals that were obtained from the camera were averaged over the active area of the detector array. The use of the diffuser did not appreciably change the conclusions, but improved the results, presumably by averaging out the polarization inhomogeneities in the source and optical elements. Since the LC retarders do not alter the beam path as their retardance is varied, the use of the diffuser should not introduce any artifacts for this type of polarimeter.

6. Calibration Procedure

The procedures described in Sections 3 and 4 require that a set of well-defined polarization states be generated to calibrate the polarimeter. These states should span all of the dimensions of the Poincaré sphere. Furthermore, it is required that the relative intensities for each state be known. It is advanta-

geous if the intensities for all of the states are the same, or at least calculable *a priori*, so that a separate measurement of intensity is not required. In the following we describe a configuration, shown in the top frame of Fig. 1, that is relatively easy to configure in a laboratory and satisfies these requirements.

We begin by generating a source of unpolarized light. We then use a polarizer and a quarter-wave retarder. The polarizer is placed in a rotation stage that in turn can be placed before [(2) in Fig. 1] or after [(1) in Fig. 1] the quarter-wave retarder. The retarder is aligned so that its fast axis is horizontal or vertical, and the polarizer is initially aligned to this direction. The signals measured by the polarimeter are then measured for a number of orientations of the polarizer placed both before and after the retarder. When the polarizer is before and after the retarder, the polarization states are given by

$$S^{\text{before}}(\theta) = [1 \quad \cos 2\theta \quad 0 \quad \sin 2\theta]^T, \tag{26}$$

$$S^{\text{after}}(\theta) = [1 \quad \cos 2\theta \quad \sin 2\theta \quad 0]^T, \tag{27}$$

respectively. Because the light incident upon the polarizer is unpolarized in both configurations, and the number of interfaces is constant (so as to have an equal amount of net reflection loss), and if the retarder has no diattenuation, the intensities for all of the reference states remain constant. These states also span the Poincaré sphere. Of course, one needs to obtain a sufficiently good source of unpolarized light, a sufficiently good polarizer, and a sufficiently accurate quarter-wave retarder. On the other hand, once one calibrates a well-characterized polarimeter, the polarimetric scale can be transferred to any other polarimeter, using a polarization state generator that may deviate substantially from the behavior given in Eqs. (26) and (27).

In our implementation, we used a tricolor light emitting diode (LED) as a source. The tricolor LED emits in three bands: red (centered on $\lambda = 630$ nm), green (centered on $\lambda = 525$ nm), or blue (centered on $\lambda = 472$ nm). The widths of the three bands were all about 25 nm, measured full width at half-maximum. By noting that there was no measureable change in the signal as the LCs were modulated, the light emitted by the LEDs was found to have no residual polarization.

For the polarizer, a dichroic polarizer was used, because these devices can be readily obtained, and many have a very good extinction coefficient (around 10^4 in the visible spectrum [24]). They also have a large open aperture and a large angular acceptance. We also have used Glan-style polarizers; the results were comparable but are not presented here. The polarizer was mounted in a manually actuated rotation stage, having a precision of about 1°.

For the retarder, we used a BK7 Fresnel rhomb. These devices are based on the phase shift of total internal reflection between the *s*- and *p*-polarized waves and are used as quasi-achromatic quarter-wave retarders [25]. The residual reflections from the faces of the rhomb are not polarization dependent, since the light is incident at normal incidence and the material is not birefringent. These devices exhibit a variation in the maximum of the relative phase of 2% in the visible spectral band. However, this phase shift can be easily determined using the Fresnel equations and knowing the Fresnel rhomb's parameters (refractive index and incident angle). Another advantage of Fresnel rhombs is that they do not rely upon accurate crystal orientation for their performance. A disadvantage of the Fresnel rhomb is that it translates the beam by a large amount. This problem is alleviated by the arrangement of the polarizer and the rhomb, whereby it is the polarizer that is rotated during the procedure rather than the rhomb, and the beam path is fixed.

The polarizer is initially aligned with respect to an auxiliary polarizer by finding the angle of maximum extinction. The retarder is then placed between the two polarizers and aligned to reattain maximum extinction. The axis of the system is thus defined by this auxiliary polarizer. In our measurements, we used the polarizer in the polarimeter (with the LC retarders removed) to set this axis. We measured the intensity for 18 different orientations (10° apart) for each of the two configurations (polarizer–rhomb and rhomb–polarizer), yielding a total of $M = 36$ reference Stokes vectors.

7. Calibration Results

Two different methods were used to calibrate the system. In the first method, it was assumed that Eq. (25) was valid, and a nonlinear least squares fit of the measured 36×6 intensities was performed allowing the six retardance values ($\delta_1 = \delta_1^a$ and δ_1^b, and $\delta_2 = \delta_2^a$, δ_2^b, δ_2^c, and δ_2^d), the three orientations of the elements (θ_1, θ_2, and θ_3), and an overall intensity to be free parameters. The other method used the algorithm described in Section 4, making no assumptions about the Mueller matrices of the polarimeter. These methods were performed for data taken for each of the three different wavelengths.

Figure 2 shows the resulting best fit to the data for the red LED ($\lambda = 630$ nm) using the first method, while Table 1 shows the best fit parameters for all three wavelengths. The data show small deviations from the theory that could not be described by the simplified description of the polarimeter. The orientation angles shown in Table 1 are all consistent with one another (the polarization optics were not moved between the measurements), but have a systematic offset of a couple degrees, presumably due to the misalignment of the polarizer and the LC modulators with respect to the reference polarization generator. The retardances also show systematic variation from their optimum values. These retardances differ from their nominal values partly due to misalignments and nonideal behavior of the elements, but mostly from the calibration data for the LC modulators being given by the manufacturer at only a single wavelength of 633 nm. Figure 3 shows the residuals of the

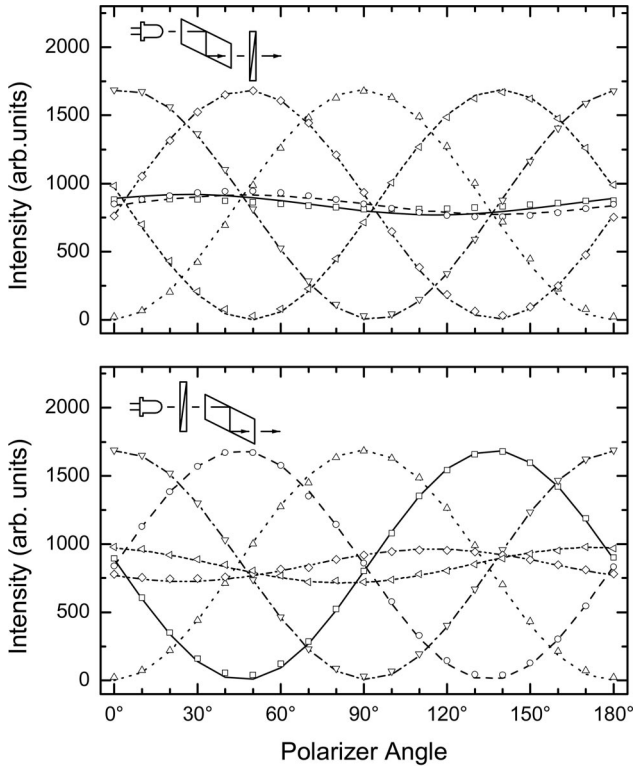

Fig. 2. Calibration data (symbols) obtained for $\lambda = 630$ nm and the best fit (curves) to the first calibration method. The top frame is for the rhomb–polarizer configuration, and the bottom frame is for the polarizer–rhomb configuration. Each of the curves corresponds to one of the six LC retardance combinations (δ_1, δ_2): (squares and solid curves) (0°, 0°), (circles and long dashed curves) (0°, −180°), (up-triangles and dotted curve) (−90°, 90°), (down-triangles and dash-dot curves) (−90°, −90°), (diamonds and dash-dot-dot curves) (0°, −90°), and (left-triangles and short-dotted curves) (0°, 90°).

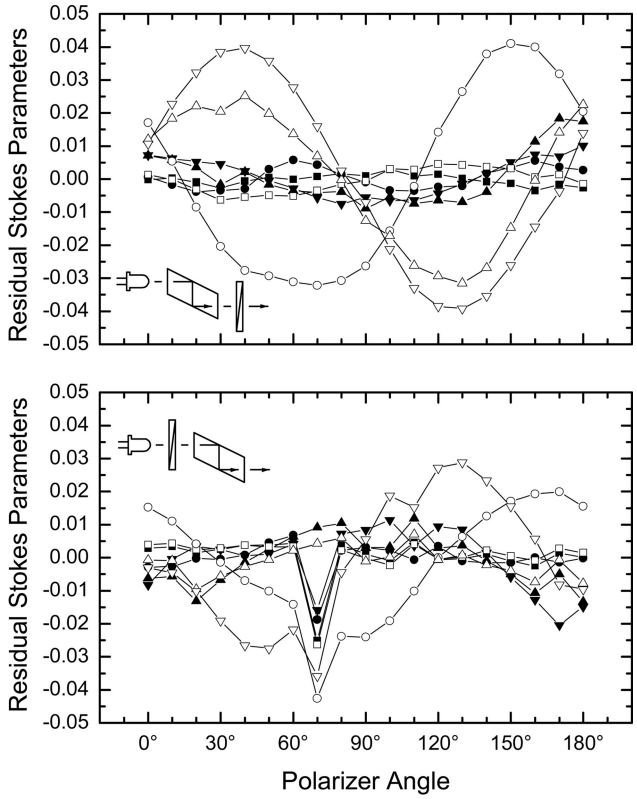

Fig. 3. Residual normalized Stokes parameters for $\lambda = 630$ nm as a function of polarizer angle. The open symbols are (squares) S_0, (circles) S_1, (up triangles) S_2, and (down triangles) S_3, for the first calibration method, and the solid symbols are respective values for the second calibration method. The top frame is for the rhomb–polarizer configuration, and the bottom frame is for the polarizer–rhomb configuration.

calibration Stokes vectors calculated by applying the data reduction matrix obtained for $\lambda = 630$ nm to the calibration data. The root mean square (rms) residuals between the reference values and the measured values for all the wavelengths are given in Table 2.

A data reduction matrix was then calculated using the second method, as described in Section 4. Figure 3 shows the calibration Stokes vectors calculated by applying the new data reduction matrix obtained for $\lambda = 630$ nm to the calibration data. Comparing the results shown in Fig. 3, we see that the resulting Stokes vectors are much closer to their reference values when we use the second method. Again, the rms residuals are given in Table 2. One can see that the second method yields rms residuals lower by at least a factor of 3. Furthermore, there is less systematic variation in the residual for the second calibration method. Note that there is one datum point in Fig. 3 that appears to be in error; this point was probably due to an

Table 1. Best-Fit Parameters Obtained from a Nonlinear Least Squares Fit to the Calibration Data

Fitted Parameter	Nominal Value	Wavelength		
		630 nm	525 nm	472 nm
θ_1	0°	2.60°	2.13°	−0.02°
θ_2	−45°	−43.75°	−43.42°	−42.12
θ_3	0°	−0.92°	−1.39°	0.61°
$\delta_1{}^a$	0°	−0.44°	−0.38°	−0.26°
$\delta_1{}^b$	−90°	−91.89°	−96.67°	−100.56°
$\delta_2{}^a$	0°	−1.50°	−0.37°	0.04°
$\delta_2{}^b$	−90°	−89.81°	−93.82°	−100.87°
$\delta_2{}^c$	−180°	−177.44°	−189.46°	−202.62°
$\delta_2{}^d$	−270°	−266.79°	−282.19°	−300.02°

Table 2. Root-Mean-Square Error of the Stokes Vector Elements based upon the Two Calibration Methods Described in the Text

	Wavelength		
Method	630 nm	525 nm	472 nm
First	0.020	0.024	0.044
Second	0.006	0.011	0.011

incorrect orientation of the polarizer during the calibration.

The calibration procedure was repeated five times to demonstrate the consistency in the matrix **W** obtained by the second procedure, using the nontruncated SVD inversion in Eq. (20) and the truncated SVD inversion in Eq. (21). The resulting matrices **W** were compared to the average of the five matrices computed using the truncated SVD inversion. The rms deviation between the matrices computed by nontruncated SVD inversion was 3.6, much larger than the mean matrix element, while that between the matrices computed by the truncated SVD inversion was 0.06. Thus, while the matrices **W** appeared unrelated to one another when the nontruncated SVD inversion was used, those calculated using the truncated SVD inversion were relatively stable and closer to the nominal matrix given in Eq. (9).

Some of the improvements in the results between the first and second methods may be a result of inaccuracy in the reference Stokes vectors. That is, the second method will force the calibration to match the reference Stokes vectors, even if the reference Stokes vectors are far from ideal. Thus, the method described is expected to yield substantially improved results when a good reference Stokes generator is available, and especially when the polarimeter itself has components that are far from ideal. Such conditions are expected in field instruments that are calibrated at a single facility.

8. Uncertainties

There are basically three types of uncertainties associated with this calibration procedure and the subsequent measurements: (a) those which are associated with uncertainties in the reference Stokes vectors, (b) those which are associated with errors in the polarimeter, and (c) those associated with the subsequent measurements. The method described in Section 3 will yield systematic uncertainties from both the reference Stokes vectors and the polarimeter. In contrast, the new method, described in Section 4, places most of the systematic uncertainties on the reference polarizations, since it makes no assumptions, other than linearity, about the elements making up the polarimeter. In this section, we discuss some of the main sources of errors and their consequences on subsequent measurements.

Errors in the reference polarizations have the effect of distorting the Poincaré sphere during subsequent measurements. As an example, Fig. 4 illustrates the effect that a retarder error has on the calibration. In the top frame, Fig. 4 shows paths in Poincaré space taken during calibration and during a subsequent measurement. Path 12 is the nominal path taken when the polarizer follows the retarder [Eq. (27)], while path 13 is that taken when the polarizer precedes the retarder [Eq. (26)]. When the actual retardance differs from $\pi/2$ by α, the plane containing the actual path (path 13′) is tilted by the same angle α. This error will cause an apparent linear distortion of the Poincaré space. The bottom frame of Fig. 4 shows the error in subsequent measurements for polarizations along a third path, path

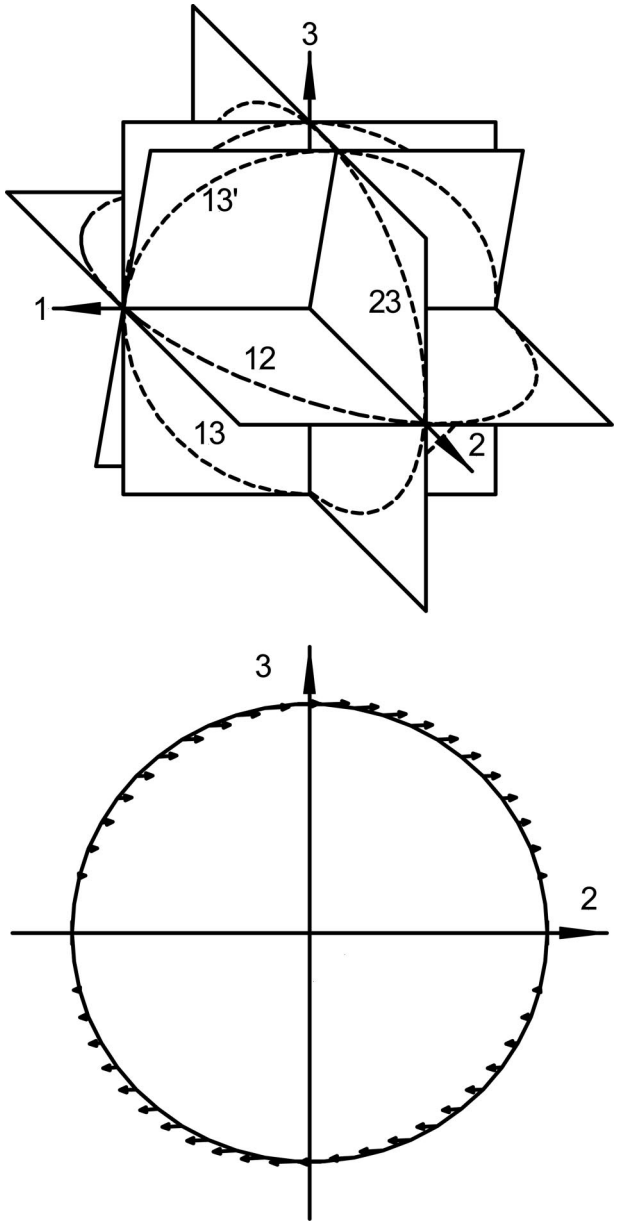

Fig. 4. Illustration of how errors in the reference polarizations affect subsequent measurements. The Poincaré space (top) shows nominal paths traced out by the reference polarizations (12 and 13). Due to an error in the retardance, nominal path 13 is actually path 13′, lying along a tilted plane. Errors in subsequent measurements for polarizations along path 23 are shown (bottom).

23. Other errors, such as those caused by a nonzero polarizer extinction coefficient or misalignment of the polarizer or retarder, will cause respective distortions of the Poincaré space and errors in one or more of the Stokes parameters. It is worth noting that points on the Poincaré sphere in the second and fourth quadrant, as shown in the bottom frame of Fig. 4, will have errors that cause them to exhibit degrees of polarization greater than one.

Another source of uncertainty results from the spectral bandwidth of the sources. Such an error occurs in the subsequent measurements and is not a result of the calibration. This uncertainty vanishes if the spectrum of the light used for calibration is the same as that arriving at the polarimeter during subsequent measurements. However, if the same light source is used to illuminate a sample, but the sample has a wavelength-dependent reflectance, errors in measured Stokes parameters will be observed. That is, the wavelengths incident on the polarimeter during calibration can differ from those incident on it during subsequent measurement. As an extreme case, we consider errors that arise when the material being studied has a large reflectance change in the middle of the spectrum of the light source. We assume that the variations in the polarimeter retardance values are inversely proportional to wavelength and that the spectrum of the source is Gaussian with a full width at half-maximum $\lambda_{\mathrm{FWHM}} = 25$ nm,

$$I(\lambda) = A \exp\left[-2.773(\lambda - \lambda_0)^2/{\lambda_{\mathrm{FWHM}}}^2\right], \qquad (28)$$

where λ_0 is the center wavelength, and A is a constant. The reflectance is then approximated by

$$R(\lambda) = \{\mathrm{erf}[(\lambda - \lambda_0)/\Delta\lambda) + 1\}/2, \qquad (29)$$

where $\Delta\lambda$ is the width of the transition. That is, $R(\lambda)$ changes from 0 to 1 over a characteristic wavelength range $\Delta\lambda$. We then simulated its effect on the calibration and subsequent measurement. First, 36 reference Stokes vectors were created. The intensities for the calibration were simulated using the LC parameters given in Table 2 and integrating the response over the source spectrum, $I(\lambda)$. The data reduction matrix was then calculated using the truncated SVD method described in Section 4. Finally, the intensities for a large number of test Stokes vectors equally spaced over the surface of the Poincaré sphere were simulated. The test Stokes vectors were obtained by integrating over the reflected spectrum, i.e., the product $I(\lambda)R(\lambda)$. The test Stokes vectors and those determined by applying the data reduction matrix to the simulated intensities were then compared. Figure 5 shows the results for the 525 nm illumination. For this specific error, the effect is largest on S_3 and least for S_1. In an extreme case, the errors in the normalized Stokes parameters from the wavelength distribution may be as large as a few percent, but in more reasonable conditions should be less than 1%.

The last sources of errors that we consider are those which are random. The reference polarization states may have errors that randomly distributed about their nominal states, and the measurements of the reference intensities and subsequent intensities will be subject to electronic and detector noise. It was found that normally distributed errors in the polarization angle with a standard deviation of 1° (an upper bound on what we expect from our manually positioned rotation stage) yield a standard error in the Stokes vector elements of about 0.5%. Presumably, if we were to use a motorized and encoded stage, this error would be insignificant (Fig. 3 exhibits a single datum, at 70° in the polarizer–rhomb configuration, that probably deviated in this manner).

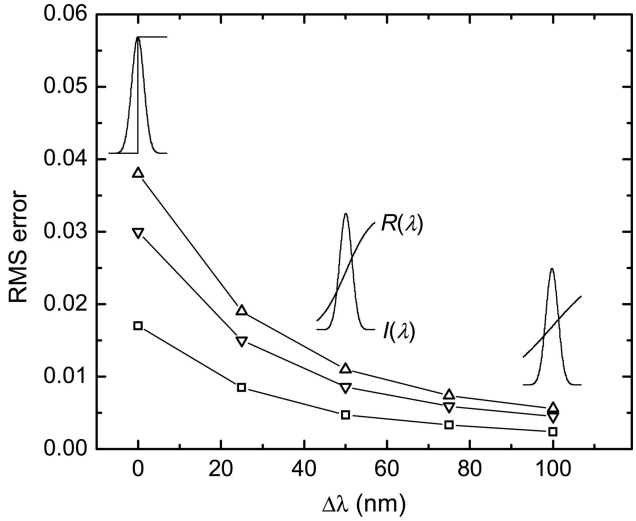

Fig. 5. Root-mean-square error in normalized Stokes parameters, (squares) S_1/S_0, (down triangle) S_2/S_0, and (up triangle) S_3/S_0, calculated as functions of the width of the reflectance edge. The insets show the spectrum $I(\lambda)$ and the reflectance $R(\lambda)$ used in the calculation for illustration.

9. Conclusion

An imaging Stokes polarimeter using of a pair of LC variable retarders and a dichroic polarizer has been described. The reference polarization states for the polarimeter calibration were generated by an unpolarized source, a polarizer, and a Fresnel rhomb, with the order of the polarizer and rhomb being interchanged. Two calibration analysis procedures were described. In the first case, assumptions were made about the optical elements in the polarimeter, and a regression analysis was used to optimize the parameters. In the second case, no assumptions about the polarimeter were made, but the data reduction matrix was obtained by a truncated SVD, keeping only the four largest singular values. The second method improved the results substantially. This method has advantages, because it can reduce the fabrication requirements of polarimeters and thus reduce their cost.

References

1. R. M. A. Azzam and N. M. Bashara, *Ellipsometry and Polarized Light* (North Holland, 1987).

2. R. A. Chipman, "Polarimetry," in *Handbook of Optics* (McGraw-Hill, 1995), Vol. 2, Chap. 22.
3. A. En Naciri, L. Johann, R. Kleim, M. Sieskind, and M. Arnann, "Spectroscopic ellipsometry of anisotropic materials: application to the optical constants of HgI_2," Appl. Opt. **38,** 647–654 (1999).
4. T. W. Cronin, E. J. Warrant, and B. Greiner, "Celestial polarization patterns during twilight," Appl. Opt. **45,** 5582–5589 (2006).
5. J. Cariou, B. Le Jeune, J. Lotrian, and Y. Guern, "Polarization effects of seawater and underwater targets," Appl. Opt. **29,** 1689–1695 (1990).
6. G. Le Brun, B. Le Jeune, J. Cariou, and J. Lotrian, "Laser imaging procedure for evaluating the polarization signature of immersed targets," Pure Appl. Opt. **2,** 445–470 (1993).
7. P. Olivard, P. Y. Gerligand, B. Le Jeune, J. Cariou, and J. Lotrian, "Measurement of optical fibre parameters using an optical polarimeter and Stokes-Mueller formalism," J. Phys. D **32,** 1618–1625 (1999).
8. F. Bentivegna, F. Boulvert, M. Guegan, B. Boulbry, A. Sharaiha, M. Tariaki, F. Pellen, B. Le Jeune, and Y. Boucher, "Polarimetric analysis of a semiconductor optical amplifier based on the Mueller–Stokes formalism," Proc. SPIE **5452,** 486–497 (2004).
9. V. Sankaran, J. T. Walsh, Jr., and D. J. Maitland, "Comparative study of polarized light propagation in biological tissues," J. Biomed. Opt. **7,** 300–306 (2002).
10. F. Boulvert, B. Boulbry, G. Le Brun, B. Le Jeune, S. Rivet, and J. Cariou, "Analysis of the depolarizing properties of irradiated pig skin," J. Opt. A: Pure Appl. Opt. **7,** 21–28 (2005).
11. P. Y. Gerligand, M. Smith, and R. Chipman, "Polarimetric images of a cone," Opt. Express **4,** 420–430 (1999).
12. O. Morel, C. Stolz, F. Meriaudeau, and P. Gorria, "Active lighting applied to three-dimensional reconstruction of specular metallic surfaces by polarization imaging," Appl. Opt. **45,** 4062–4068 (2006).
13. P. J. Wu and J. T. Walsh, Jr., "Stokes polarimetry imaging of rat tail tissue in a turbid medium: degree of linear polarization image maps using incident linearly polarized light," J. Biomed. Opt. **11,** 014031 (2006).
14. J. S. Tyo and T. S. Turner, Jr., "Variable-retardance, Fourier-transform imaging spectropolarimeters for visible spectrum remote sensing," Appl. Opt. **40,** 1450–1458 (2001).
15. J. S. Tyo, D. L. Goldstein, D. B. Chenault, and J. A. Shaw, "Review of passive imaging polarimetry for remote sensing applications," Appl. Opt. **45,** 5453–5469 (2006).
16. J. S. Tyo, "Noise equalization in Stokes parameter images obtained by use of variable-retardance polarimeters," Opt. Lett. **25,** 1198–1200 (2000).
17. J. S. Tyo, "Design of optimal polarimeters: maximization of signal-to-noise ratio and minimization of systematic error," Appl. Opt. **41,** 619–630 (2002).
18. D. H. Goldstein and R. A. Chipman, "Error analysis of a Mueller matrix polarimeter," J. Opt. Soc. Am. A **7,** 693–700 (1990).
19. B. Boulbry, B. Le Jeune, B. Bousquet, F. Pellen, J. Cariou, and J. Lotrian, "Error analysis and calibration of a spectroscopic Mueller matrix polarimeter using a short-pulse laser source," Meas. Sci. Technol. **13,** 1563–1573 (2002).
20. G. H. Golub and C. F. Van Loan, *Matrix Computations* (Johns Hopkins U. Press, 1983), Chap. 2, pp. 11–29.
21. W. H. Press, S. A. Teukolsky, W. T. Vetterling, and B. P. Flannery, *Numerical Recipes in C* (Cambridge University Press, 1992), Chap. 2, pp. 59–71.
22. B. Boulbry, T. A. Germer, and J. C. Ramella-Roman, "A novel hemispherical spectro-polarimetric scattering instrument for skin lesion imaging," Proc. SPIE **6078,** 128–134 (2006).
23. B. Laude-Boulesteix, A. De Martino, B. Drévillon, and L. Schwartz, "Mueller polarimetric imaging system with liquid crystals," Appl. Opt. **43,** 2824–2832 (2004).
24. S. Huard, *Polarization of Light* (Wiley, 1997).
25. R. J. King, "Quarter-wave retardation systems based on the Fresnel rhomb principle," J. Sci. Instrum. **43,** 617–622 (1966).